IEEE Access
Multidisciplinary | Rapid Review | Open Access Journal

Received 23 August 2023, accepted 21 October 2023, date of publication 25 October 2023, date of current version 1 November 2023.

*Digital Object Identifier 10.1109/ACCESS.2023.3327465*

RESEARCH ARTICLE

# DC Series Arc Failure Diagnosis Using Artificial Machine Learning With Switching Frequency Component Elimination Technique

**HOANG-LONG DANG[1], SANGSHIN KWAK[1], (Member, IEEE), AND SEUNGDEOG CHOI[2], (Senior Member, IEEE)**

[1]School of Electrical and Electronics Engineering, Chung-Ang University, Seoul 06974, South Korea
[2]Department of Electrical and Computer Engineering, Mississipi State University, Starkville, MS 39762, USA

Corresponding authors: Sangshin Kwak (sskwak@cau.ac.kr) and Seungdeog Choi (seungdeog@ece.msstate.edu)

This work was supported in part by the National Research Foundation of Korea (NRF) funded by the Korean Government, Ministry of Science and ICT (MSIT), under Grant 2020R1A2C1013413; and in part by the Korea Electric Power Corporation under Grant R21XO01-3.

**ABSTRACT** The intricate spectrum of arc faults elicited by diverse load types introduces a complex and formidable challenge in residential series arc fault detection. Series DC arc faults pose a significant concern as they can potentially instigate fire incidents and exert adverse ramifications on power systems if left undetected. Nonetheless, their detection within practical power systems remains challenging, predominantly attributed to the meager arc current magnitude, the absence of a discernible zero-crossing interval, and the manifestation of multifarious aberrant behaviors contingent upon the diverse array of power loads and controllers. Importantly, the conventional safeguards, notably encompassing protection fuses, may exhibit inefficacy in promptly activating during the occurrence of series DC arc faults. The ramifications of undiscerned arc faults are profound, with the potential for engendering erroneous operational modes within power systems, thereby amplifying the risk of material and human casualties. In light of these exigencies, the development of an efficacious detection mechanism targeting series arc faults within DC systems becomes a paramount imperative. This research proposed a preprocessing signal to eliminate the switching noises, which could degrade the performance of artificial machine learning algorithms. The diagnosis results valid the effectiveness of the proposed diagnosis scheme for all ranges of switching frequencies.

**INDEX TERMS** DC arc failure, switching noise elimination, machine learning.

## I. INTRODUCTION

The classical grid infrastructure was formulated based on fossil fuel-driven power generation, a prominent contributor to environmental degradation. This circumstance has engendered a surge in attention and capital allocation towards renewable energy sources (RES), exemplified by photovoltaic (PV) and wind power technologies. These sustainable alternatives stand poised as robust contenders in the quest for harnessing environmentally benign energy resources [1], [2]. As a result, the integration of grid-connected RES has recently experienced a substantial surge, with a growing application trend observed in residential settings and power distribution networks [3]. Furthermore, there is a growing concern for the safety aspects of RES and the associated grid-connected inverters. Notably, RES inherently manages DC power, which introduces the potential risk of DC arc faults occurring between the PV panels and the inverters [4]. Within a DC power system, the potential emergence of a fault arc can stem from multiple sources, including the aging of the electrical line insulation, the slackening of electrical connections, the presence of humid air, or a sudden surge in voltage or current. These DC fault arcs wield significant influence in the initiation of electrical fires, thereby underscoring their relevance in the domain of electrical safety. Consequently, the exploration and enhancement of DC fault arc detection technology assumes paramount importance in the pursuit of bolstering the safety standards of DC power systems [5].

The associate editor coordinating the review of this manuscript and approving it for publication was Tariq Masood.

The creation of electric arcs transpires through ionization within air gaps existing between conductors, constituting a prevalent occurrence in AC as well as DC systems. The manifestation of series arc faults is rooted in factors such as the vibration of weakened or loosened terminal connections, disruptions within electrical circuits, the natural aging of cables, wear and tear on conductive components, suboptimal upkeep practices, exposure to aircraft fluids, and the influence of chemicals [6], [7]. Unlike AC systems, where arcs can cease during the natural current zero-crossing points within the sinusoidal cycle, DC systems lack zero-crossings, potentially prolonging arcs. These persistent arcs in DC systems can pose a threat if not adequately addressed. The magnitude of the arc fault current is usually lesser than the customary operational current owing to the inclusion of a series impedance introduced by the formation of the arc itself. This scenario poses a significant hurdle, as traditional overcurrent protection approaches demonstrate their inadequacy in detecting and isolating series arc faults within DC systems [8], [9]. Prior studies have yielded various algorithms to identify instances of DC series arc faults. Notably, time domain analysis, as demonstrated in [5], [10], and [11], has been harnessed to discern arc fault conditions by leveraging data related to current and voltage. While these approaches offer swift detection capabilities coupled with uncomplicated circuitry and algorithms, their vulnerability to switching noise and load fluctuations is a notable limitation. Within the literature, frequency analysis methodologies have been deployed for the identification of arc fault conditions, as evident in [12] and [13]. These approaches center around the utilization of techniques such as the fast Fourier transform (FFT) or the short-time Fourier transform, allowing for the extraction of distinctive features characterizing arc fault scenarios within the frequency domain. Earlier investigations have delved into multi-resolution analysis supplemented by adaptable window functions. However, the effectiveness of arc fault detection through frequency domain analysis is intricately linked to the judicious selection of frequency bandwidth [14]. Notably, the conventional detection range typically spans several tens of kilohertz, a range that can potentially undermine detection accuracy due to the influence of inverter-induced switching noise. Machine learning-driven approaches have been increasingly harnessed in contemporary research endeavors to ascertain and diagnose faults. These methodologies have exhibited their utility in arc fault diagnosis [15], [16], [17], [18]. The scholarly community has adeptly employed these sophisticated techniques within the DC arc fault diagnosis context, leading to notable and affirmative outcomes. In this research, the combination between the switching noise elimination technique and artificial machine learning was employed to diagnose the DC arc fault. First, within every sampling interval, the arc current signal is derived and subsequently subjected to FFT analysis. This analytical process facilitates the extraction and computation of the pertinent frequency range associated with the specific characteristic. Then, the filtering process is executed to eliminate the switching frequency noise [19]. After that, the signal after the filtering process is transformed into the final feature and behaves as the input of artificial machine learning (AML). The diagnosis results prove the effectiveness of the proposed detection scheme and increase the detection accuracy, especially in the cases of low switching frequency. The structure of this paper unfolds subsequently. Section II delves into the configuration of the experimental apparatus, elucidating alterations in current characteristics across time and frequency domains within both normal and arcing phases. In Section III, an elaborate exposition ensues concerning the AML algorithms employed for the detection of arc faults, coupled with an exploration of switching noise filtering techniques in the context of this investigation. Section IV systematically presents the outcomes of the arc fault detection process facilitated by the utilization of four AML algorithms and combining them with the filtering technique. This is undertaken across scenarios involving diverse current amplitudes and operational frequencies. Ultimately, the summative deductions and insights gleaned from the AML-driven arc fault detection are encapsulated within Section V, concluding this study.

## II. HARDWARE SETUP AND ARC CHARACTERISTICS

### A. HARDWARE SETUP

Figure 1 portrays the schematic representation elucidating the acquisition of DC arc data. The data acquisition was orchestrated in adherence to the tenets outlined in UL1699B [20], shaping the design of the arc-generating circuit. The deliberate separation of the arc rods initiated the arc, with the subsequent deployment of an oscilloscope to capture the current trajectories traversing the rods both before and following the arcing event. The ensuing analysis of the arc currents was effectuated through the MATLAB computational environment. The experimental framework dedicated to arc generation encompassed a confluence of essential components, including a DC power supply, arc generator, and loads. Notably, the experimental paradigm incorporated the utilization of an N8741A DC power supply sourced from Keysight Technologies, USA. As illustrated in Figure 1, the load was subjected to a controlled DC voltage. Upon this, activation of the step motor, interlinked with the arc rods, initiated their controlled separation. To ensure meticulous data capture, an oscilloscope (Tektronix MSO3054, USA) was deployed, operating at a sampling frequency of 250 kHz. The vital role of data acquisition was vested in Tektronix TCP312 (Tektronix, OR, USA), serving as the current probe facilitating accurate arc current measurement. The ambit of analysis for DC arc fault embraced both temporal and spectral domains. The exploration further encompassed the systematic generation of DC arcs across diverse experimental scenarios, facilitating comprehensive data accrual. These experimental conditions are comprehensively cataloged in Table 1.

Figure 1(c) illustrates the architectural configurations of the three-phase inverter units which were harnessed as the predominant loads within the confines of this research

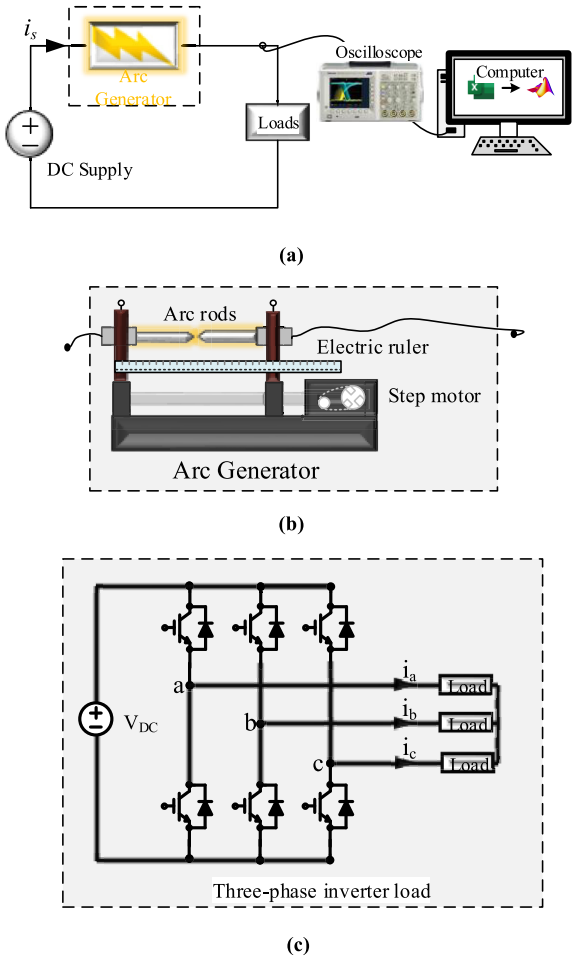


**FIGURE 1.** Hardware setup. (a) DC arc circuit. (b) Arc generator. (c) Three-phase inverter load.

**TABLE 1.** Specifications of the hardware setup.

| Experimental specifications | Values |
|---|---|
| Supply voltage | 300 V |
| Switching frequencies ($f_{swi}$) | 5, 10, 15, 20 kHz |
| Sampling frequency ($f_{sam}$) | 250 kHz |
| Current amplitudes | 5, 8 A |
| Inverter resistor load | 10 Ω |
| Inverter inductor load | 10 mH |

endeavor. The operational essence of these inverters resides in the conversion of DC signals into AC signals, engendering a dynamic whereby solely a solitary switch remains engaged within each phase leg during any discrete temporal juncture. This systematic arrangement begets a repertoire of eight distinct switching vectors, germane to the holistic operation of the three-phase inverter apparatus. In the present investigation, the orchestration of these inverter units was deftly steered through the prism of space vector modulation, a sophisticated modulation technique unfurled to exert precision control over the pulsating width modulation. Within this ambit, the overarching aspiration encompassed the manipulation of a prescribed DC voltage, adroitly commanding the disposition of six discrete switches to eminently replicate

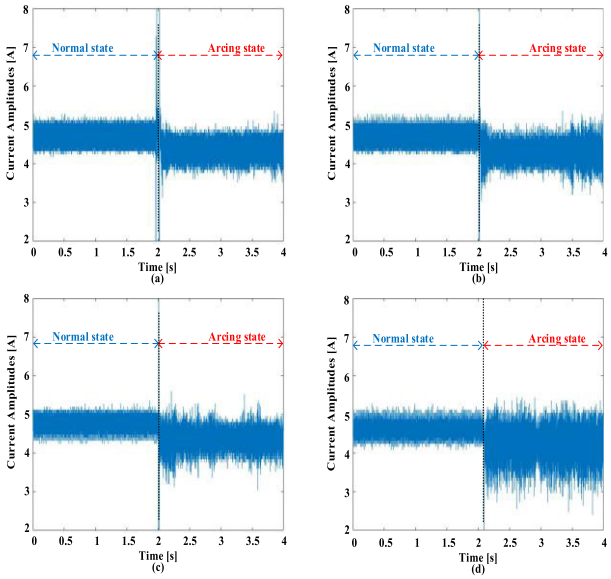


**FIGURE 2.** Current signals for different switching frequencies at 5 A current amplitude. (a) 5 kHz. (b) 10 kHz. (c) 15 kHz. (d) 20 kHz.

the sinusoidal waveforms emblematic of a three-phase AC system, affording leeway for the judicious calibration of both frequency and amplitude attributes.

### B. ARC CHARACTERISTICS

Figure 2 provides a visual representation of the waveforms corresponding to both the normative and arcing states, each evoked at varying switching frequencies whilst maintaining a current amplitude of 5A. Evident across the diverse switching frequencies is the consonance in waveform configuration antecedent to the inception of arcing. However, upon the eventuation of an arc, a panoply of anomalous behaviors crystallizes within the waveforms. This constellation encompasses an augmentation in harmonic constituents concomitant with the load current, a metamorphosis in the waveform profile of the load current engendering distortion, and a marginal diminution in the amplitude of the prevailing current. The initial phase of arcing is invariably demarcated by conspicuous spikes in amplitude, a salient manifestation underpinned by the incendiary discharge of electrical sparks. Notably, the scale of these electrical sparks accords variance, commensurate with the spectrum of switching frequencies in deployment. It is germane to acknowledge that these conspicuous aberrant phenomena proffer cogent prospects for harnessing them as discriminative elements in the ambit of arc fault detection.

After this, a meticulous dissection of the current signals anterior and posterior to the arc occurrence is undertaken, with a specific focus on their spectral characteristics facilitated through FFT analysis. To ensure granularity, the dataset is compartmentalized into discrete subsets, each subjected to individualized FFT scrutiny. The outcome of this process culminates in the configuration of each set embodying a compendium of 500 data points, acquired at a resolute sampling rate of 250 kHz.

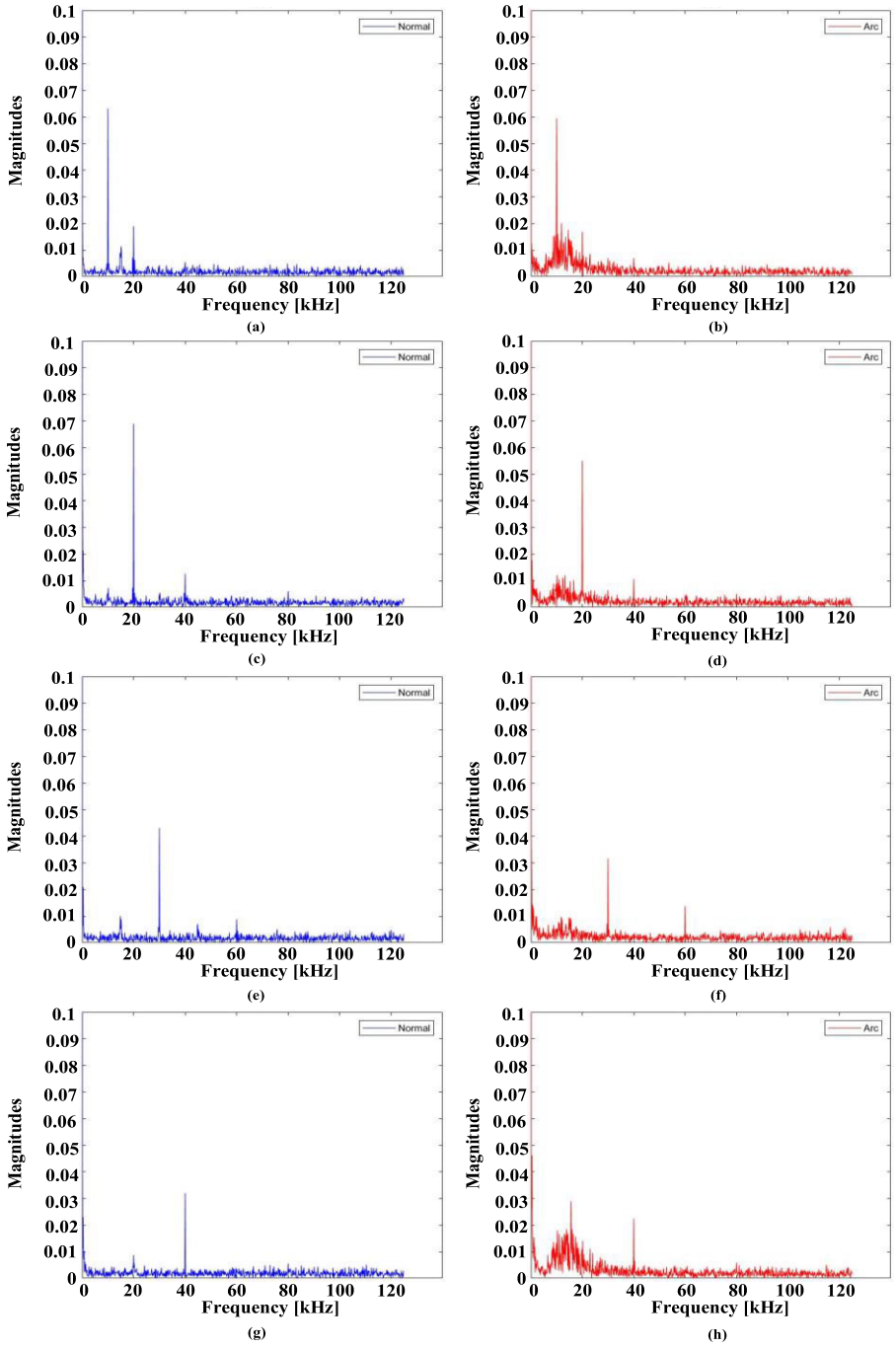


**FIGURE 3.** FFT analysis of current before and after arc at 5 A and different switching frequencies. (a) Normal state at 5 kHz. (b) Arcing state at 5 kHz. (c) Normal state at 10 kHz. (d) Arcing state at 10 kHz. (e) Normal state at 15 kHz. (f) Arcing state at 15 kHz. (g) Normal state at 20 kHz. (h) Arcing state at 20 kHz.

As portrayed in Figure 3, the outcomes of the FFT analysis, executed afore and after the arc incidence, are graphically elucidated across a constellation of scenarios where the current amplitude is fixed at 5 A, each corresponding to distinct switching frequencies encompassing 5, 10, 15, and 20 kHz. Remarkably, the depicted spectral profiles in Figure 3 substantiate the conspicuous absence of any FFT distortion anterior to the arc initiation, a pervasive phenomenon spanning all investigated switching frequency regimes. Furthermore, a scrutinizing examination of the frequency profiles in Figure 3 postulates the intriguing observation of concentrated switching noise manifesting exclusively within the vicinities of the prescribed switching frequency bands. This discloses a riveting revelation where, at a switching frequency of 5 kHz, the spectral landscape is conspicuously punctuated by a nucleus of switching noise that resolutely

envelops the frequency bands of 5, 10, 15, and 20 kHz. Analogous revelations reverberate through the panorama of other investigated switching frequencies, wherein the concentration of switching noise gravitates invariably towards harmonics and multiples thereof, aligning synchronously with the corresponding switching frequency magnitudes. Conversely, a disparate pattern emerges after the occurrence of the arc, characterized by a discernible array of distortions encapsulated within the frequency spectrum spanning from approximately 3 kHz to 30 kHz across all switching frequency spectrums. Evidently, a pronounced concentration of switching frequency-induced noise manifests close to the multiples of the respective switching frequencies. Nonetheless, a nuanced observation emerges wherein certain diminutive instances of switching frequency-induced noise, pervading the expanse of 3 kHz to 30 kHz, intersect and conflate with the arc-induced distortions, thereby coalescing and intricately intermingling within this frequency range.

## III. SWITCHING FREQUENCY NOISE ELIMINATION TECHNIQUE AND ARTIFICIAL MACHINE LEARNING

### A. SWITCHING FREQUENCY NOISE ELIMINATION TECHNIQUE

The methodology employed for the mitigation of switching frequency noise operates within the confines of the frequency domain, leveraging the sampled arc current signals. This approach is designed to amplify the efficacy of characteristic extraction, effectuate judicious filtering, and ultimately enhance the precision of fault identification. The principal objective of the characteristic extraction process is to discern and extract the inherent attributes encompassing the DC series arc fault current. Meanwhile, the filtration process is instrumental in accentuating the salient frequency components intrinsic to the arc current signal. The switching frequency noise elimination (SFNE) technique contains two stages. The first stage extracts the concerning frequency components located in the specific frequency range. The second stage filters the switching noise of the extracted frequency components and evaluates the final feature for the input of AML.

#### 1) FREQUENCY COMPONENT EXTRACTION

During each discrete sampling period, the arc current signal is isolated and subsequently subjected to FFT analysis. This analytical procedure facilitates the identification and computation of the pertinent characteristic frequency range. The frequency resolution ($f_{res}$) and the enumeration of frequency components are denoted by (1) and (2), respectively, wherein $f_{sam} = 250$ kHz represents the sampling frequency and $N = 500$ sampling points contained within each sampling interval.

$$f_{res} = \frac{f_{sam}}{N} \tag{1}$$

$$\text{enumeration of frequency components} = \frac{N}{2}. \tag{2}$$

**TABLE 2. Specifications of the frequency ranges.**

| Frequency ranges | 1st component | Final component | Total components |
|---|---|---|---|
| FR1(3 – 30 kHz) | 6th | 60th | 54 |
| FR2(3 – 45 kHz) | 6th | 90th | 84 |
| FR3(3 – 60 kHz) | 6th | 120th | 114 |
| FR4(3 – 80 kHz) | 6th | 160th | 154 |

Through the application of each FFT operation, a set of 500 frequency components is generated, each possessing a frequency resolution of 500 Hz. In the scope of this investigation, four distinct frequency ranges are utilized to assess the impact of frequency variation. These designated frequency ranges, along with the corresponding count of frequency components within each range, are systematically delineated in Table 2. As an illustration, the frequency components spanning from the 6th to the 60th position are indicative of the frequency range spanning 3 kHz to 30 kHz. As evident from Figure 3, the distortions arising from the arc occurrence are positioned within the frequency spectrum of 3 kHz to 30 kHz, consistently across all switching frequencies. Consequently, the initiation of the four designated frequency ranges (FRs) is set at 3 kHz, ensuring a comprehensive encompassment of all arc-related distortions.

#### 2) FILTERING SWITCHING FREQUENCY NOISE

The primary objective underlying the process of eliminating switching frequency noise is to supplant the noise content concentrated around the multiples of the switching frequency. Let $FR_x$ denote the $x^{th}$ frequency component within any given FR, and $FR_{avr}$ represent the arithmetic mean of the corresponding FR. In instances where the magnitude of $FR_x$ exceeds that of $FR_{avr}$ by a factor of three, $FR_x$ alongside the two adjacent frequency components prior and after $FR_x$, are reassigned the value of $FR_{avr}$. This reassignment process is systematically applied to all current components, adhering to the aforementioned criteria, and it is reiterated until no frequency components surpass three times the magnitude of $FR_{avr}$. This iterative sequence constitutes the procedure termed as switching frequency noise elimination.

Illustrated in Figure 4 is the successful application of SFNE at a current amplitude of 5 A and a switching frequency of 5 kHz for the band FR2. The previously observed switching frequency noises around 10, 15, and 20 kHz have been effectively eliminated in both normal and arcing states. As a result of this noise elimination process, the signals exhibit improved clarity, and the arc distortions are more distinctly discernible. This advancement in signal quality holds the potential to enhance the feature extraction process for arc diagnosis. Likewise, the implementation of the SFNE method was executed for a current amplitude of 5 A at a switching frequency of 10 kHz for the band FR2, as depicted in Figure 5. In this case, the previously observed switching frequency interferences around 10, 20, 30, and 40 kHz have been effectively removed. Consequently, the resulting signals manifest clarity in both the normal and arcing states. Similar outcomes

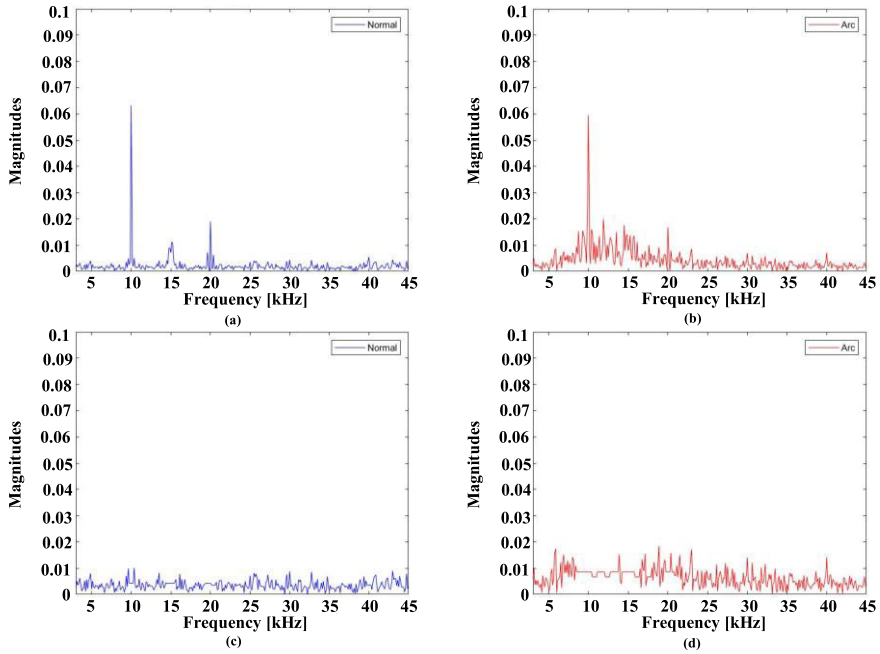


**FIGURE 4.** Switching frequency noise elimination at a current amplitude of 5 A and a switching frequency of 5 kHz for the band FR2. (a) Frequency components before noise filtering at normal state. (b) Frequency components before noise filtering at arcing state. (c) Frequency components after noise filtering at normal state. (d) Frequency components after noise filtering at normal state.

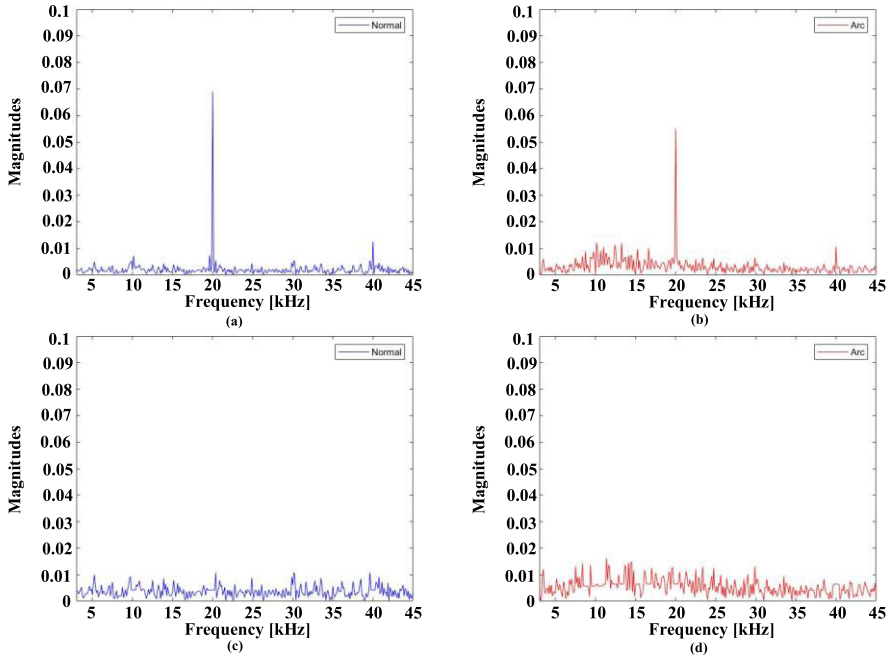


**FIGURE 5.** Switching frequency noise elimination at a current amplitude of 5 A and a switching frequency of 10 kHz for the band FR2. (a) Frequency components before noise filtering at normal state. (b) Frequency components before noise filtering at arcing state. (c) Frequency components after noise filtering at normal state. (d) Frequency components after noise filtering at normal state.

are achieved across other scenarios, where the switching frequency disturbances are effectively attenuated, leading to enhanced signal visibility. As a consequence, the discernibility of arc distortions is significantly improved, facilitating their more accurate detection.

### *B. ARTIFICIAL MACHINE LEARNING*

Figure 6 illustrates the theoretical framework and configuration of several AML models. The K-Nearest Neighbor (KNN) algorithm is rooted in the assumption that entities possessing analogous attributes are likely to be positioned

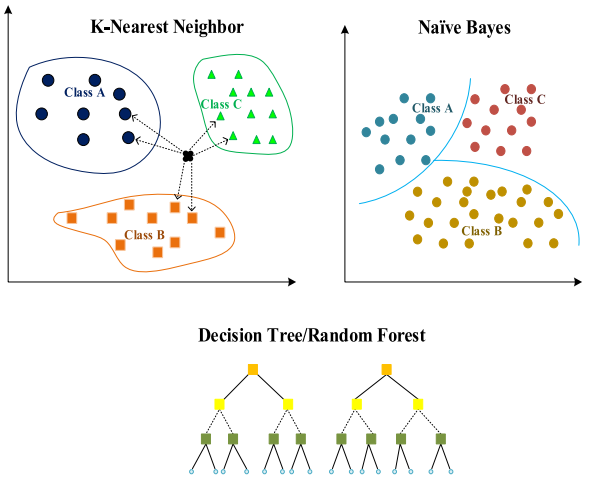


**FIGURE 6.** Theoretical framework and configuration of several AML models.

in close proximity. Stated differently, similar objects exhibit spatial adjacency within the same cluster [21]. The Decision Tree (DT), a versatile methodology, serves both classification and regression tasks. Its nomenclature implies a structure resembling a tree, akin to a flowchart, that delineates predictions stemming from a sequence of feature-based partitions. The process commences at a root node and culminates in a verdict rendered at the terminal nodes [22]. The Random Forest (RF), as the name implies, constitutes an ensemble of discrete decision trees. This forest of trees collectively contributes to predictions. Each constituent tree generates a class prediction, and the class with the highest efficiency becomes the model's prediction [23]. The Naïve Bayes (NB) classifiers encompass a set of classification algorithms grounded in Bayes' theorem. Although not a solitary algorithm but rather a collection of algorithms, they are united by the shared principle of the independence between each pair of features undergoing classification [24].

## IV. DC ARC FAULT DIAGNOSIS WITH SWITCHING FREQUENCY NOISE ELIMINATION AND ARTIFICIAL MACHINE LEARNING

Figure 7 presents the block diagram depicting the envisaged framework for arc fault diagnosis. The prevailing current data is subjected to sampling and subsequently segmented into subdatasets, each consisting of 500 data points. These individual data subsets undergo FFT analysis, following which their FFT-derived data enter a two-stage process aimed at eliminating switching frequency noise. In the first stage, distinct frequency components within specific FRs are extracted. Subsequently, the technique of SFNE is applied, resulting in the acquisition of the definitive feature. This extracted feature is employed as an input for AML in the context of DC arc fault diagnosis, spanning both the training and testing phases. The data distribution ratio between normal and arc instances is maintained at a 1:1 proportion for both the training and testing stages. For the assessment of the efficacy of AML algorithms, the accuracy metric serves as the primary evaluative criterion. The accuracy detection rate denotes the proportion of accurately predicted data sets with the overall count of test data sets. It is expressed as

$$\%\ of\ Accuracy = \frac{\#\ of\ correct\ predicted\ data\ set}{\#\ of\ total\ test\ data\ sets}. \quad (3)$$

Figure 8 portrays the results of the diagnostic procedure at a current amplitude of 5 A within FR1 across various switching frequencies. Remarkably, all AML algorithms augmented with the SFNE technique exhibit exceptional performance in contrast to their counterparts lacking SFNE integration. Particularly noteworthy is the significant contribution of the SFNE approach to the remarkable achievements of AML algorithms at a 5 kHz switching frequency. In general, the diagnostic accuracies rise in correspondence with the increase in switching frequency. Figure 9 delineates the diagnostic outcomes at an 8 A current amplitude within FR1 across distinct switching frequencies. The conspicuous trend is that AMLs incorporating SFNE consistently showcase remarkable performance when compared to their non-SFNE counterparts. Moreover, the SFNE technique substantially amplifies the diagnostic capabilities of AML algorithms at a switching frequency of 20 kHz. Within FR1, the undeniable effectiveness of the SFNE technique is evident, as it consistently attains impressive levels of accuracy in detecting arc faults across diverse AML models. This increase in accuracy is noted with the augmentation of switching frequency, regardless of whether the SFNE technique is employed or not.

Figure 10 presents the diagnostic outcomes within FR2 at a current amplitude of 5 A across various switching frequencies. Remarkably, all AML algorithms enhanced with the SFNE technique demonstrate exceptional performance when compared to their counterparts lacking SFNE integration for all switching frequencies of 5 kHz, 10 kHz, 15 kHz, and 20 kHz. Furthermore, the SFNE strategy significantly contributes to the remarkable achievements of AML algorithms at switching frequencies of 15, and 20 kHz. Figure 11 provides insight into the diagnostic results at an 8 A current amplitude within FR2, considering different switching frequencies. Clearly, the AMLs incorporating SFNE consistently exhibit outstanding performance when contrasted with their non-SFNE counterparts at a switching frequency of 10 kHz. These results underscore the unmistakable efficacy of the SFNE technique within FR2, consistently achieving remarkable levels of accuracy across various AML models for the detection of arc faults. Similar to FR1, the diagnosis accuracies increase with the increase of switching frequency whether the SFNE technique is adopted or not.

Figure 12 illustrates the diagnostic results within FR3 at a current amplitude of 5 A under various switching frequencies. All AML algorithms enhanced with the SFNE technique showcase exceptional performance when contrasted with their non-SFNE counterparts for all switching frequencies. Additionally, the accuracies of all AML algorithms with SFNE strategy slightly decrease compared with FR1 (Figure 8) and FR2 (Figure 10) especially at 5 kHz

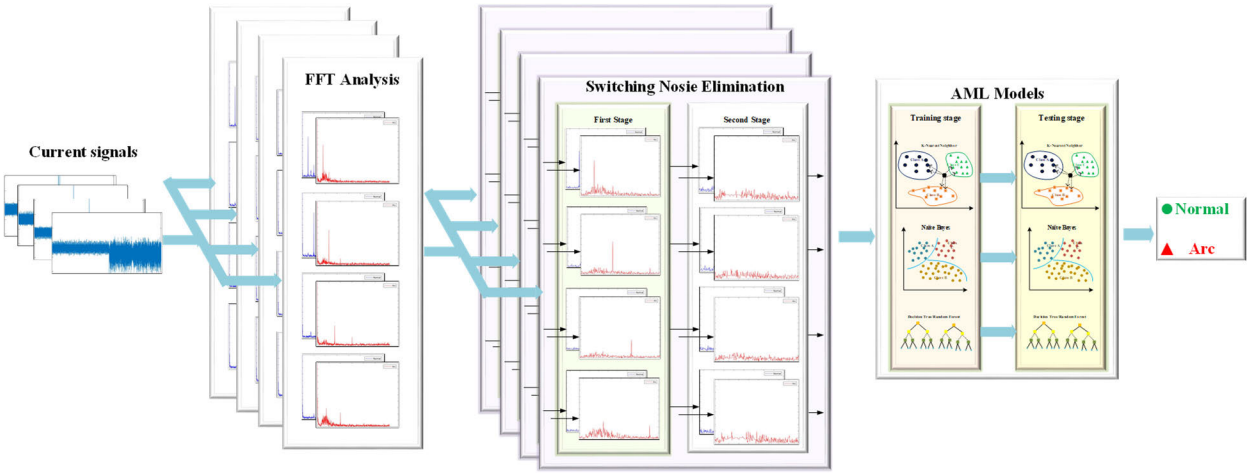


**FIGURE 7.** Proposed DC arc diagnosis scheme.

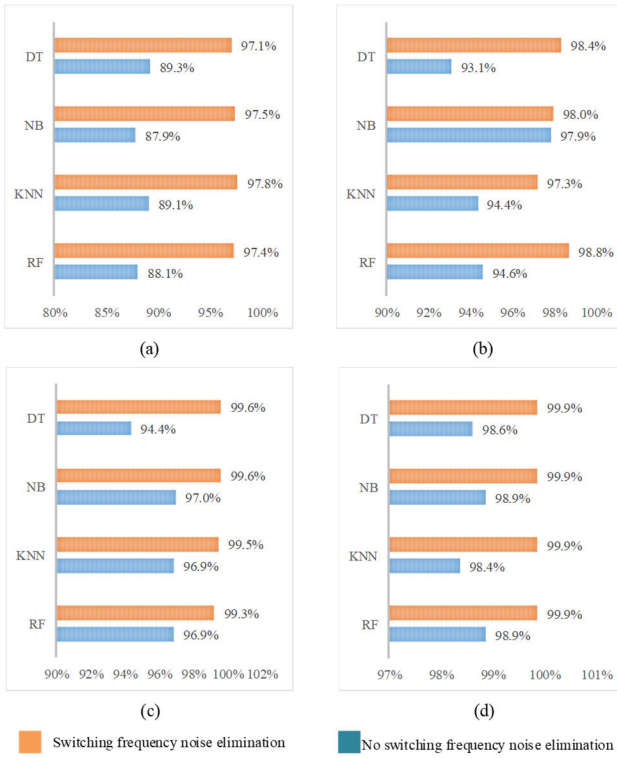


**FIGURE 8.** DC arc diagnosis results at 5 A current amplitude in FR1 under different switching frequencies. (a) 5 kHz. (b) 10 kHz. (c) 15 kHz. (d) 20 kHz.

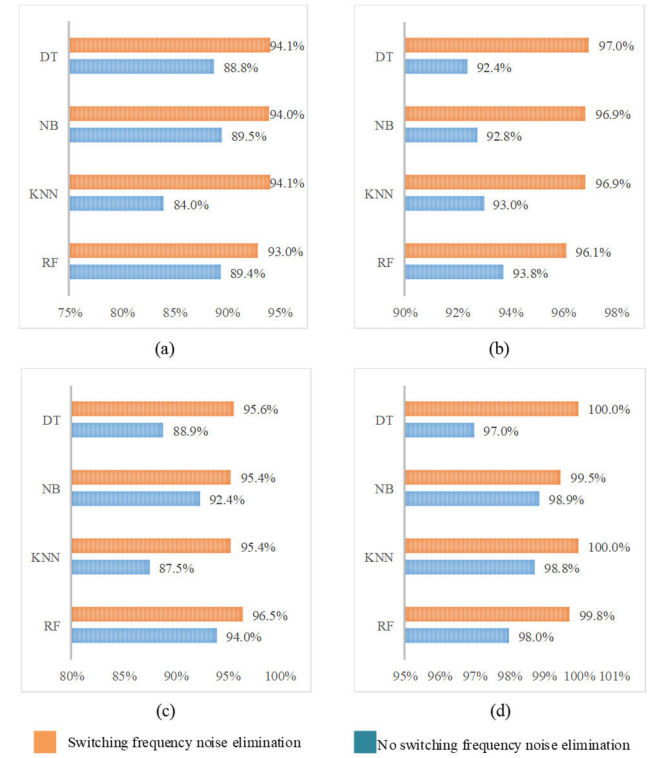


**FIGURE 9.** DC arc diagnosis results at 8 A current amplitude in FR1 under different switching frequencies. (a) 5 kHz. (b) 10 kHz. (c) 15 kHz. (d) 20 kHz.

switching frequency. Figure 13 provides a comprehensive view of the diagnostic outcomes at an 8 A current amplitude within FR3, considering different switching frequencies. AMLs incorporating SFNE consistently have higher performance when compared with their non-SFNE counterparts across switching frequencies of 5 kHz, 10 kHz, 15 kHz, and 20 kHz. However, the difference in accuracies with and without the SFNE technique of AML algorithms is reduced compared with FR1 (Figure 9) and FR2 (Figure 11) for all switching frequencies. These results underscore the effectiveness of the SFNE technique within FR3, achieving higher levels of accuracy across diverse AML models for detecting arc faults.

Figure 14 presents the diagnostic outcomes within FR4 at a current amplitude of 5 A across a spectrum of switching frequencies. For all ranges of switching frequencies, all AML algorithms enhanced with the SFNE technique demonstrate exceptional performance in contrast to their non-SFNE counterparts. However, the differences in accuracies of AML algorithms are insignificant at 20 kHz switching frequency.

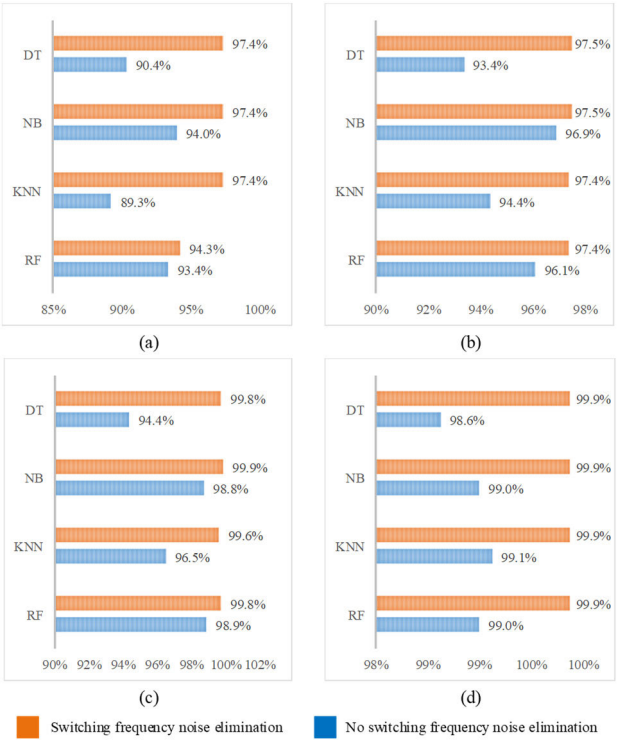


**FIGURE 10.** DC arc diagnosis results at 5 A current amplitude in FR2 under different switching frequencies. (a) 5 kHz. (b) 10 kHz. (c) 15 kHz. (d) 20 kHz.

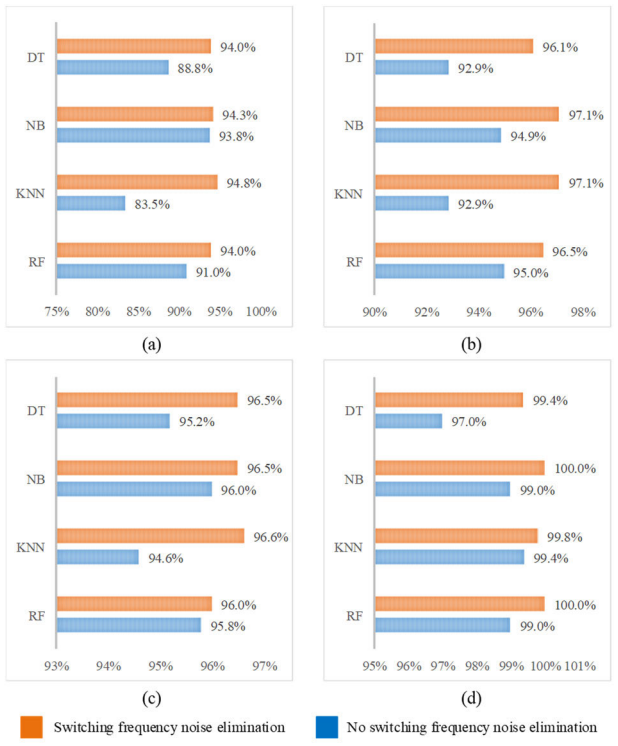


**FIGURE 11.** DC arc diagnosis results at 8 A current amplitude in FR2 under different switching frequencies. (a) 5 kHz. (b) 10 kHz. (c) 15 kHz. (d) 20 kHz.

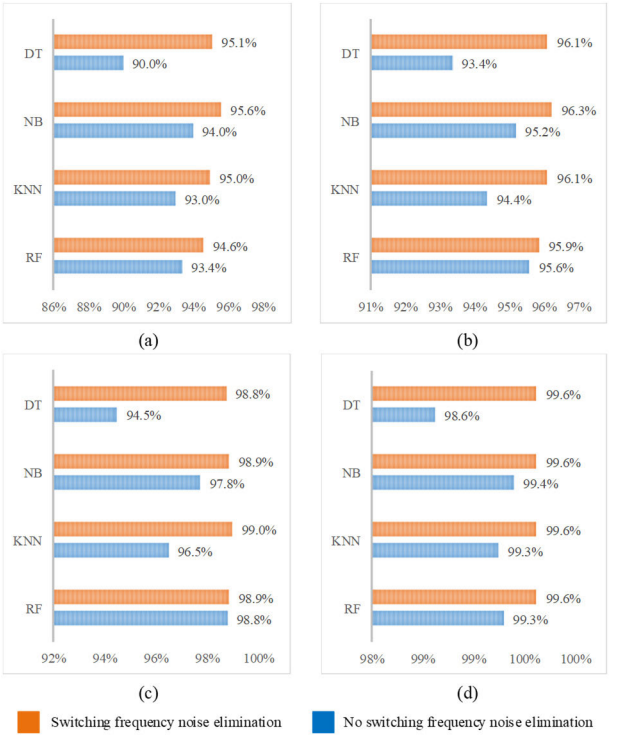


**FIGURE 12.** DC arc diagnosis results at 5 A current amplitude in FR3 under different switching frequencies. (a) 5 kHz. (b) 10 kHz. (c) 15 kHz. (d) 20 kHz.

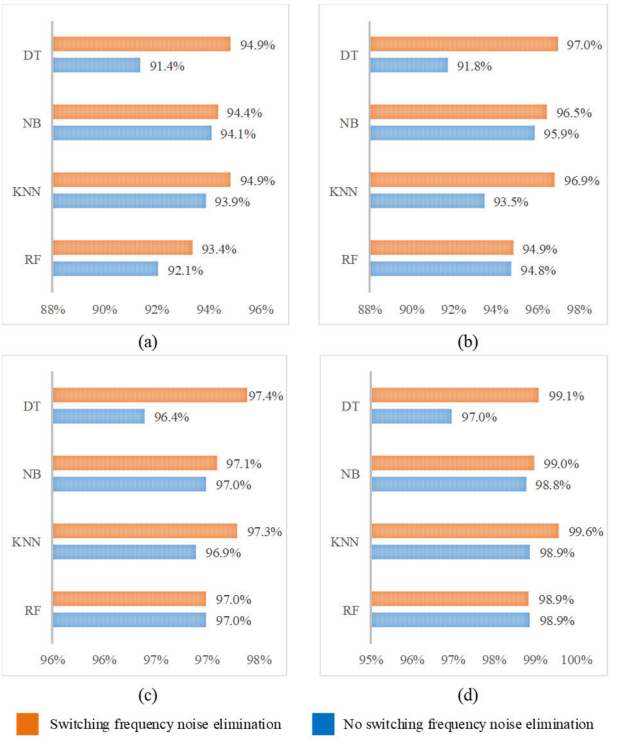


**FIGURE 13.** DC arc diagnosis results at 8 A current amplitude in FR3 under different switching frequencies. (a) 5 kHz. (b) 10 kHz. (c) 15 kHz. (d) 20 kHz.

Similarly, Figure 15 offers a comprehensive perspective on the diagnostic outcomes at an 8 A current amplitude within FR4, considering various switching frequencies. The evidence is clear that AMLs incorporating SFNE consistently

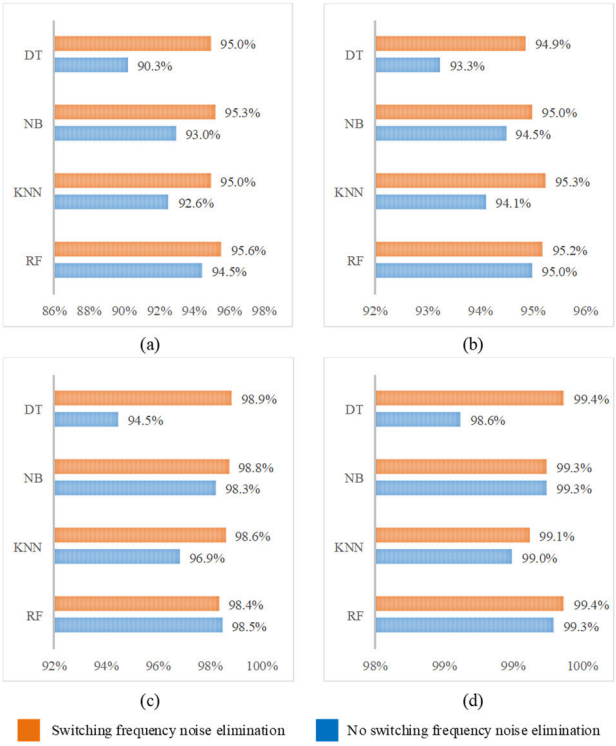


**FIGURE 14.** DC arc diagnosis results at 5 A current amplitude in FR4 under different switching frequencies. (a) 5 kHz. (b) 10 kHz. (c) 15 kHz. (d) 20 kHz.

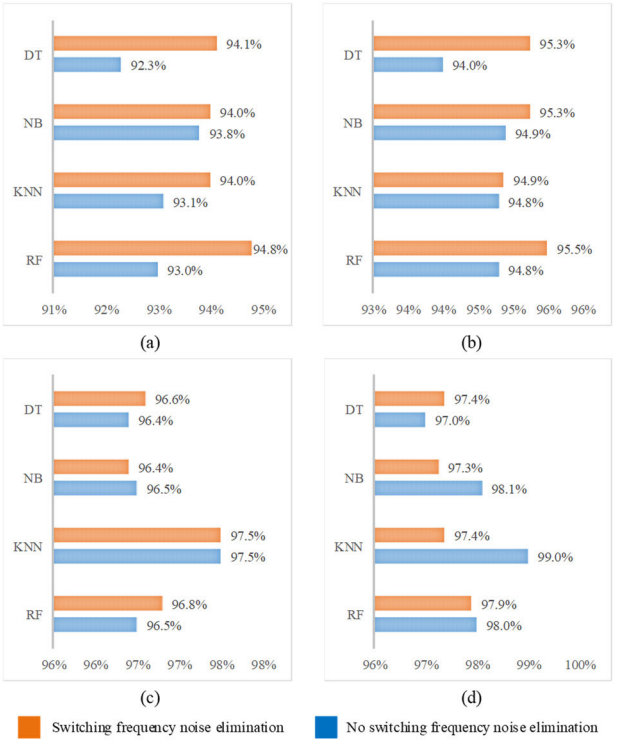


**FIGURE 15.** DC arc diagnosis results at 8 A current amplitude in FR4 under different switching frequencies. (a) 5 kHz. (b) 10 kHz. (c) 15 kHz. (d) 20 kHz.

showcase slightly higher performance when juxtaposed with their non-SFNE counterparts across switching frequencies of 5 kHz, 10 kHz, 15 kHz, and 20 kHz. Furthermore, the accuracies of all AML algorithms with the SFNE technique in FR4 are not high as the AML with SFNE in FR1, FR2, and FR3, especially at switching frequency of 20 kHz. These results emphasize the effectiveness of the SFNE technique within FR4, consistently achieving higher levels of accuracy across diverse AML models for the detection of arc faults.

Figure 16 depicts the mean accuracies concerning both switching frequencies and frequency ranges. An observable trend is the rise in accuracies as switching frequency increases, whether or not the SFNE technique is applied. This escalation in switching frequency has the potential to augment the informative content within each dataset, thereby contributing to accuracy enhancement. The efficacy of the proposed diagnostic scheme in enhancing arc fault detection rates across all frequency ranges is evident. Among these, FR1 stands out as the most successful. As elaborated in Figure 3, the bulk of arc distortions is concentrated within the 3 kHz to 30 kHz range, rendering the disparities between normal and arcing states in FR1 more distinct compared to other frequency ranges. Additionally, the amplitude of switching frequency noises diminishes at higher frequencies. By implementing the SFNE technique in FR3 and FR4, these noises are largely sieved out at lower frequencies. Consequently, the SFNE technique's performance experiences a slight reduction in FR3 and FR4. Figure 17 illustrates the mean accuracies of AML across the four FRs. When employing the SFNE technique, disparities in the accuracy of AML algorithms are negligible. RF and NB emerge as the top-performing AML algorithms, consistently achieving the highest performance levels, regardless of the presence of the SFNE technique.

The outcomes of the diagnostic evaluations across all FRs affirm the effectiveness of the proposed arc detection scheme integrated with the SFNE technique in significantly enhancing the accuracy rates of all AML models, particularly at lower switching frequencies. At higher switching frequencies, the performance disparity between AML models with and without the SFNE technique in terms of accuracy is not substantial.

## V. CONCLUSION

This research introduces an innovative strategy for detecting DC arc faults by integrating the SFNE technique with AML models. Irrespective of the switching frequency, the distortions arising from arc occurrences consistently inhabit the frequency range of 3 kHz to 30 kHz. Consequently, in order to encompass full arc-related distortions, the chosen FRs should span this spectrum. With the application of the SFNE procedure, there is a notable enhancement in signal clarity, leading to a more pronounced and distinct manifestation of arc distortions. This improvement in signal quality has the potential to elevate the efficacy of feature extraction methods in arc diagnosis. The diagnostic results validate the efficiency of the proposed detection scheme, particularly in augmenting


**FIGURE 16.** Average accuracies regarding different switching frequencies and frequency ranges.

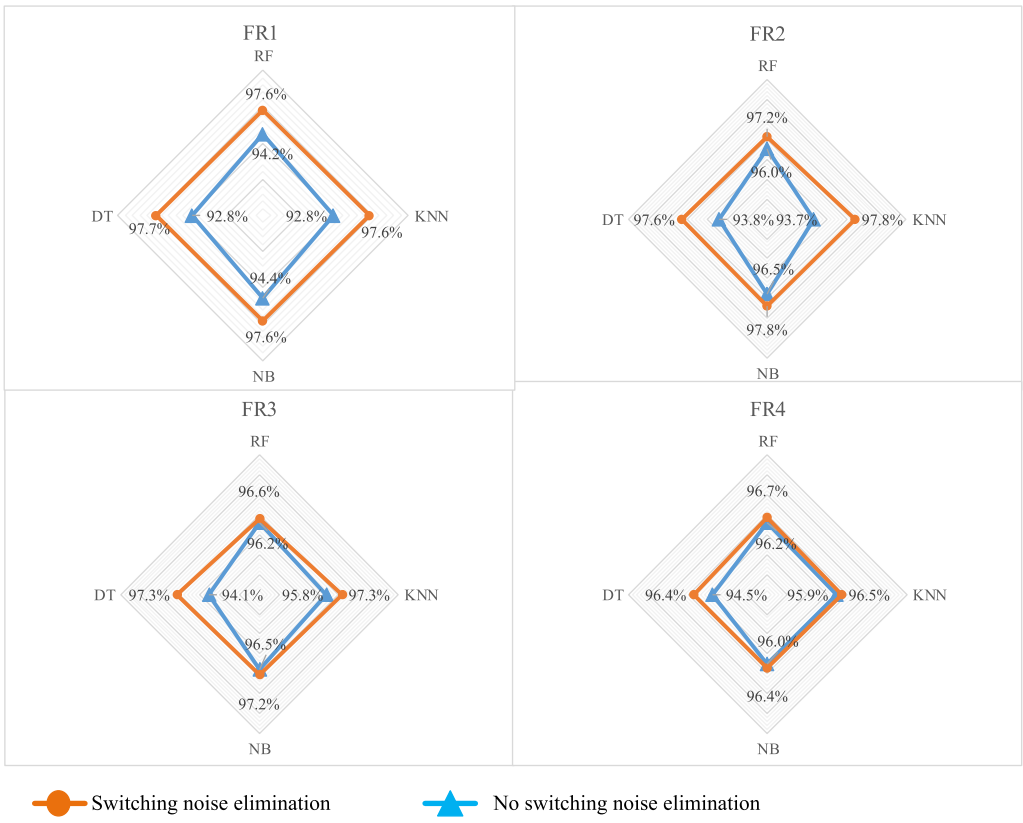


**FIGURE 17.** Average accuracies of AML algorithms under different frequency ranges.

detection accuracy at low switching frequencies. This outcome can be attributed to the fact that arc distortions primarily localize within the 3 to 30 kHz frequency range. At lower switching frequencies, the coexistence of switching noise and

arc distortion frequency components can result in performance deterioration. By mitigating this overlap, the SFNE technique contributes to improved diagnostic performance. RF and NB emerge as consistently high-performing AML algorithms, achieving top-tier performance levels. The diagnostic evaluations across all FRs corroborate the effectiveness of the proposed arc detection scheme when integrated with the SFNE technique, notably enhancing the accuracy rates of all AML models, particularly at lower switching frequencies.

## REFERENCES


[1] H.-P. Park and S. Chae, "DC series arc fault detection algorithm for distributed energy resources using arc fault impedance modeling," *IEEE Access*, vol. 8, pp. 179039–179046, 2020.

[2] Y. Ding, T. Ma, and Y. Zhou, "Integration of renewable energy sources in modern power grids: Challenges and opportunities," *Energies*, vol. 13, no. 2, p. 406, 2020.

[3] J. Shen, C. Jiang, Y. Liu, and X. Wang, "A microgrid energy management system and risk management under an electricity market environment," *IEEE Access*, vol. 4, pp. 2349–2356, 2016.

[4] I. Hassan, A. Haddad, M. Al-Dhaifallah, R. Al-Muhaidib, A. Al-Muhaidib, H. Al-Nuaim, and N. Al-Mutairi, "Investigating the impact of smart inverter-enhanced anti-islanding protection on islanding detection performance," *Energies*, vol. 13, no. 19, p. 5217, 2020.

[5] Q. Lu, Z. Ye, M. Su, Y. Li, Y. Sun, and H. Huang, "A DC series arc fault detection method using line current and supply voltage," *IEEE Access*, vol. 8, pp. 10134–10146, 2020.

[6] B. C. Brusso, "History of aircraft wiring arc-fault protection [history]," *IEEE Ind. Appl. Mag.*, vol. 23, no. 3, pp. 6–11, May 2017.

[7] R. Landfried, M. Boukhlifa, T. Leblanc, P. Teste, and J. Andrea, "Stability, spatial extension extinction of an electric arc in aeronautical conditions of pressure under 540 V DC," *Eur. Phys. J. Appl. Phys.*, vol. 87, no. 30901, pp. 1–9, Sep. 2019.

[8] S. Dhar, R. K. Patnaik, and P. K. Dash, "Fault detection and location of photovoltaic based DC microgrid using differential protection strategy," *IEEE Trans. Smart Grid*, vol. 9, no. 5, pp. 4303–4312, Sep. 2018.

[9] V. Psaras, Y. Seferi, M. H. Syed, R. Munro, P. J. Norman, G. M. Burt, R. Compton, K. Grover, and J. Collins, "Review of DC series arc fault testing methods and capability assessment of test platforms for more-electric aircraft," *IEEE Trans. Transport. Electrific.*, vol. 8, no. 4, pp. 4654–4667, Dec. 2022.

[10] N. L. Georgijevic, M. V. Jankovic, S. Srdic, and Z. Radakovic, "The detection of series arc fault in photovoltaic systems based on the arc current entropy," *IEEE Trans. Power Electron.*, vol. 31, no. 8, pp. 5917–5930, Aug. 2016.

[11] G. Bao, R. Jiang, and X. Gao, "Novel series arc fault detector using high-frequency coupling analysis and multi-indicator algorithm," *IEEE Access*, vol. 7, pp. 92161–92170, 2019.

[12] S. Chae, J. Park, and S. Oh, "Series DC arc fault detection algorithm for DC microgrids using relative magnitude comparison," *IEEE J. Emerg. Sel. Topics Power Electron.*, vol. 4, no. 4, pp. 1270–1278, Dec. 2016.

[13] S. Chen, X. Li, and J. Xiong, "Series arc fault identification for photovoltaic system based on time-domain and time-frequency-domain analysis," *IEEE J. Photovolt.*, vol. 7, no. 4, pp. 1105–1114, Jul. 2017.

[14] S. Lu, T. Sirojan, B. T. Phung, D. Zhang, and E. Ambikairajah, "DA-DCGAN: An effective methodology for DC series arc fault diagnosis in photovoltaic systems," *IEEE Access*, vol. 7, pp. 45831–45840, 2019.

[15] H.-L. Dang, S. Kwak, and S. Choi, "Different domains based machine and deep learning diagnosis for DC series arc failure," *IEEE Access*, vol. 9, pp. 166249–166261, 2021.

[16] H.-L. Dang, S. Kwak, and S. Choi, "Parallel DC arc failure detecting methods based on artificial intelligent techniques," *IEEE Access*, vol. 10, pp. 26058–26067, 2022.

[17] H.-L. Dang, S. Kwak, and S. Choi, "Identifying DC series and parallel arcs based on deep learning algorithms," *IEEE Access*, vol. 10, pp. 76386–76400, 2022.

[18] H.-L. Dang, J.-C. Kim, S. Kwak, and S. Choi, "Analysis and diagnosis scheme of parallel arc failure in DC power lines," *J. Electr. Eng. Technol.*, vol. 18, no. 3, pp. 1851–1862, May 2023.

[19] J.-C. Gu, D.-S. Lai, J.-M. Wang, J.-J. Huang, and M.-T. Yang, "Design of a DC series arc fault detector for photovoltaic system protection," *IEEE Trans. Ind. Appl.*, vol. 55, no. 3, pp. 2464–2471, May 2019.

[20] *Outline of Investigation for Photovoltaic (PV) DC Arc-Fault Circuit Protection*, Standard UL 1699B, Underwriters Laboratories, Inc., Northbrook, IL, USA, 2013.

[21] T. Cover and P. Hart, "Nearest neighbor pattern classification," *IEEE Trans. Inf. Theory*, vol. IT-13, no. 1, pp. 21–27, Jan. 1967.

[22] L. Breiman, J. Friedman, R. Olshen, and C. Stone, *Classification and Regression Trees* (Statistics/Probability Series). Belmont, CA, USA: Wadsworth and Brooks, 1984.

[23] L. Breiman, "Random forests," *Mach. Learn.*, vol. 45, no. 1, pp. 5–32, 2001.

[24] P. Langley, W. Iba, and K. Thompson, "An analysis of Bayesian classifiers," in *Proc. 10th Nat. Conf. Artif. Intell.*, 1992, pp. 223–228.


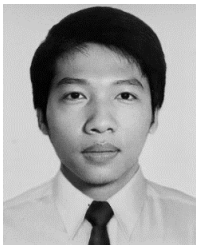

**HOANG-LONG DANG** received the B.S. degree in electrical and electronics engineering from the Ho Chi Minh City University of Technology, Vietnam, in 2015. He is currently pursuing the combined M.S. and Ph.D. degrees in electrical and electronics engineering with Chung-Ang University, Seoul, South Korea. His research interests include matrix converters, fault detections, and artificial intelligence.

**SANGSHIN KWAK** (Member, IEEE) received the Ph.D. degree in electrical engineering from Texas A&M University, College Station, TX, USA, in 2005. From 2007 to 2010, he was an Assistant Professor with Daegu University, Gyeongsan, South Korea. Since 2010, he has been with Chung-Ang University, Seoul, South Korea, where he is currently a Professor. His current research interests include the design, modeling, control, and analysis of power converters for electric vehicles and renewable energy systems and the prognosis and fault tolerant control of power electronics systems.

**SEUNGDEOG CHOI** (Senior Member, IEEE) received the B.S. degree in electrical and computer engineering from Chung-Ang University, Seoul, South Korea, in 2004, the M.S. degree in electrical and computer engineering from Seoul National University, Seoul, in 2006, and the Ph.D. degree in electric power and power electronics from Texas A&M University, College Station, TX, USA, in 2010. From 2006 to 2007, he was a Research Engineer with LG Electronics, Seoul. From 2009 to 2012, he was a Research Engineer with Toshiba International Corporation, Houston, TX, USA. From 2012 to 2018, he was an Assistant Professor with The University of Akron, Akron, OH, USA. Since 2018, he has been an Associate Professor with Mississippi State University, Starkville, MS, USA. His current research interests include degradation modeling, fault tolerant control, fault tolerant design of electric machines, power electronics, batteries, solar panels, and wider vehicular/aircraft microgrid systems.